Wireless Personal Communications (2021) 117:2495–2511
https://doi.org/10.1007/s11277-020-07991-y

A Simple Shape Descriptor Merging Arithmetical Wrap Around Technique with Absolute Localized Pixel Differences

Kethepalli Mallikarjuna[1] · **Bepar Abdul Raheem**[2] · **Govindaraj Pathanadka**[3] · **Sudhakar Mogappair Suriyakumar**[4]

Accepted: 11 November 2020 / Published online: 28 November 2020

Abstract

The quest for computationally simple, highly accurate and precise shape descriptors supporting retrieval continues to be an active research area in computer vision. In this paper, a simple feature descriptor is realized by blending Modulo Arithmetic (MA) with Local Absolute Pixel Differences (LAPD) labelled as MA-LAPD. MA initially refines edges of images through modulo normalization and later operated by LAPD to capture local texture patterns. Subsequently, LAPD encodes the local intensity transitions in eight directions with regard to center pixel. The two prominent directional indices are converted into unique decimal codes that represent each pixel position, thus, transforming each image into a collection of LAPD codes. The ensuing LAPD image is then fabricated into histograms for characterizing the distribution of local features, used for matching and retrieval. Quantitative and qualitative investigations on Kimia's 99, MPEG-7 Part-B and Tari-1000 datasets reveal consistent Bull's Eye Retrieval (BER) scores above 91%. Also, relative analysis exposes the superiority of MA-LAPD with its predecessors in majority of the datasets.

Keywords Bull's eye retrieval · Image histogram · Local absolute pixel differences · Modulo arithmetic · Shape retrieval

✉ Kethepalli Mallikarjuna
kethepallimallikarjuna@rgmcet.edu.in

Bepar Abdul Raheem
Prof.abdulrahim.1969@ieee.org

Govindaraj Pathanadka
govindaraj.p@iitg.ac.in

Sudhakar Mogappair Suriyakumar
sudhakar.ms@vit.ac.in

1 RGM College of Engineering and Technology, Nandyala, India

2 Annamacharya Institute of Technology and Sciences, Rajampet, India

3 AJ Institute of Engineering and Technology, Manglore, Mangalore, India

4 Vellore Institute of Technology, Vellore, India

1 Introduction

Shape recognition and classification fields of computer vision highly rely on shape for feature characterization and description. Also, the size of the resulting descriptor can be reduced by defining it in terms of the shape feature. Moreover, shape descriptors abiding invariance are deemed fit for applications such as image and video retrieval, image segmentation and recognition [1].

The inherent characteristic of human visual system interprets images as geometrical shapes by visual decomposition. Further, shapes offer the ability to discern the variations within intra and interclasses. Prevailing shape matching and retrieval schemes offered escalated results over the years by covering affine transformations such as translation, scaling and rotation. Whilst, achieving such quality in shape matching is challenging and cumbersome especially in cases of non-linear deformations. Moreover, the complexity increases with increase in multiple deformations. This necessitates the need for a shape descriptor with acute distinguishing abilities warranting improved shape matching and retrieval. Also, the development of light, acute shape-based characterization methods aims to bring down the complexity involved in its realization.

Scores of image retrieval schemes reported in literature are aimed at escalating the scheme's accuracy, retrieval rate. Primarily, these schemes are categorized as Contour, region-based that are further parted into global, structural for representing shapes [2]. Global method extracts shapes from integral boundaries by disintegrating and defining them. The merits and demerits of such available descriptors are chronologically listed below in brief.

Capitulating contour points by spatially correlating a point with its neighbours resulted in the shape context (SC) [3] descriptor. The spatial distribution of the acquired contour points were then transformed into a sixty dimension histogram. Ling et al. [4] blended inner shape distances across different scales to produce the articulation invariant multidimensional scaling (MDS) shape descriptor. Euclidean metric in [3] was replaced with the shortest path algorithm for determining the distances amongst the contour points followed by dynamic programming to yield a novel shape descriptor. Global shape characterization schemes [5, 6] configure boundary points by employing signed areas of triangles at different scales labelled as triangle area representation (TAR). They capture the curvature of contour points and their polarities determine its concavity or convexity. The global descriptor of Souza et al. [7] evaluated the Hough transform statistics from the object neighbourhood to build the Hough Transform Statistics neighbourhood (HTSn). While Srestasathiern et al. [8] localised shapes in conic-regions and the extracted coefficients were, piecewise approximated from the conic basis. The projective conic invariants were then accumulated to yield the feature histogram. The above descriptors were built by considering the entire image as a shape entity.

Whilst the local descriptors neglect regions containing lesser shape details for formulating feature descriptors. Accordingly, Wu et al. [9] captured shape features employing lower-order invariant Tchebichef moments. Likewise, shape features from common base triangles were spatially extracted by Hu et al. [1] to formulate feature vectors named as Common Base Triangle Area (CBTA). The resulting vertices were later modified and shape matching was performed using dynamic programming. Likewise, Circle Views (CVs) [10] silhouetted shapes by applying Fourier transform to CV signatures. Similarly, salient feature points from the images were compacted into Shape contours [11] and matching was achieved by dynamic programming. The shape methodology of Kaothanthong et al. [12]

evaluated the Distance Interior Ratio (DIR) by acquiring the line intersection patterns and their distribution to build the shape histogram. Off late, shape descriptors were employed for investigating and detecting cracks in integrated circuits embossed on Printed Circuit Boards (PCB) [13] under different color spaces. Likewise, [14] suggested a shape descriptor that spectrally distinguished non-road objects and road interconnections. The recent shape retrieval approach [15, 16] employed semantic images and clustering technique for achieving an improved retrieval rate.

Despite accomplishing improved performances, the aforementioned schemes fused the computationally intensive dynamic programming or more complex modules into their retrieval phase that increased their computational aspects. Also, these approaches either fall under the local or global paradigm whereas the offered descriptor merges the local variations across spatial scales in an overlapping fashion to realize a local–global shape histogram. Hence, this scheme deploys light computational models for realizing shape descriptors offering improved retrieval efficacy, thereby, excelling its competitors. Therefore, simple Modulo Arithmetic and Local Absolute Pixel Differences in image subregions were utilized for characterizing shapes and later concatenated into feature histograms. Investigation on diverse popular shape datasets namely MPEG7-Part B, Tari-1000 and Kimia's 99 reveal the supremacy of the presented descriptor in terms of the Bull's Eye Retrieval (BER).

The remainder of the paper is systematized as: Sect. 2 elaborates in detail the MA-LAPD feature extraction procedure. Experimental results and subsequent validation with current state-of-art systems upon publicly available shape image databases is performed and discussed in Sect. 3. A brief outline of the future work with regard to the presented descriptor is concluded in Sect. 4.

2 MA-LAPD Descriptor

Schemes targeting higher retrieval performance heavily rely on shape characterization to produce descriptors with high discerning abilities. This paper delivers one such shape descriptor confirming the aforementioned criteria. Initially, MA is applied over each 3×3 sub-region, followed by LAPD and this procedure is iterated throughout the entire image. The resulting LAPD features are then packed into feature vectors. This process is repeated on the entire image database in the offline mode and the yielded descriptors are stacked along with the respective images. Then the K-Nearest Neighbour (KNN) algorithm exploits the spatial relationship of the feature database for shape classification. During the online phase, the extracted shape of the query is compared with the feature database and the near identical ones are retrieved according to the matched shapes. The related shapes are ranked based on the matching criteria and displayed. A diagrammatic overview of the retrieval scheme is presented in Fig. 1, and the detailing of the diverse modules is discussed in below sections.

2.1 Modulo (Wrap-Around) Arithmetic

The introduced feature extraction scheme treats images as a square geometrical object. Subsequently, every image is resized to $M \times M$ dimension using the bilinear interpolation to produce fixed length features. The modified image is then tiled into 3×3 regions and MA operates on each sub-region with the modulo value determined by the mean of the

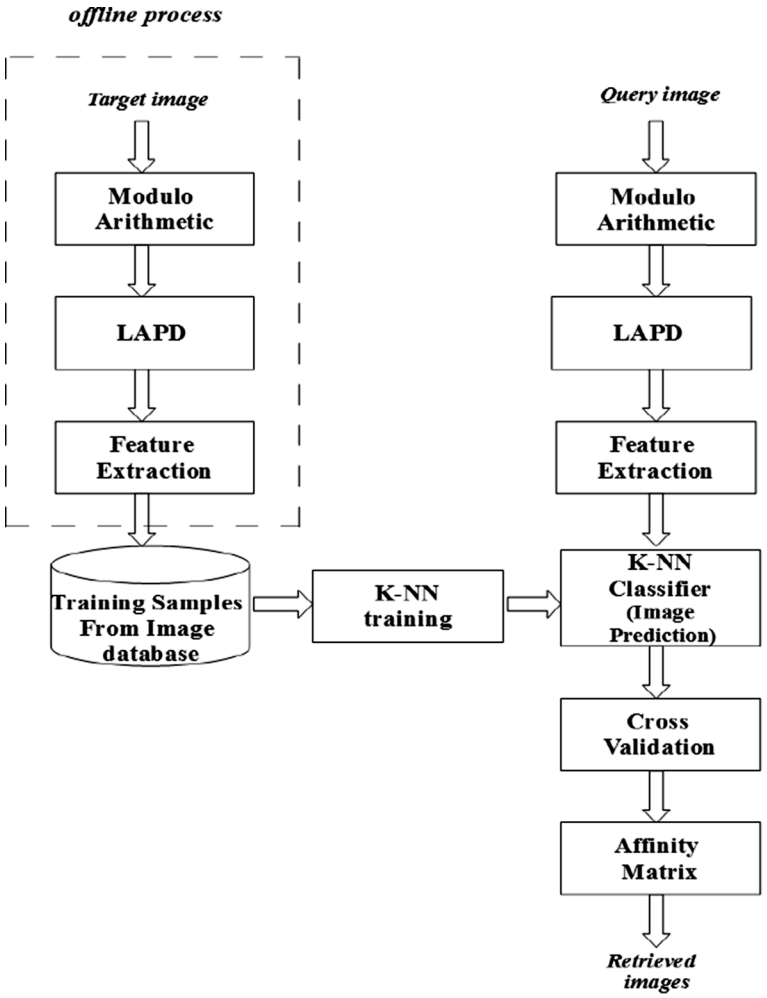

Fig. 1 Overall outline of the intended work

sub-region in an overlapping fashion. This arrangement enforces congruency amongst the pixel values by localisation (modulo) of high frequency data for enriching the fine features. The above discussed process is outlined in Fig. 2.

2.2 Local Absolute Pixel Difference (LAPD) Encoding

Later a novel direction-based feature encoding scheme is introduced by exploiting the absolute pixel differences of each sub-region. LAPD encodes the local textural and intensity transitions of each image pixel into a compact feature descriptor attained at minimal cost. Consequently, LAPD evaluates the absolute pixel differences of a neighbourhood region with regard to the center pixel. Later, the extremes of the pixel differences determine the directional pixel indices that undergo maximum intensity variations. These prominent

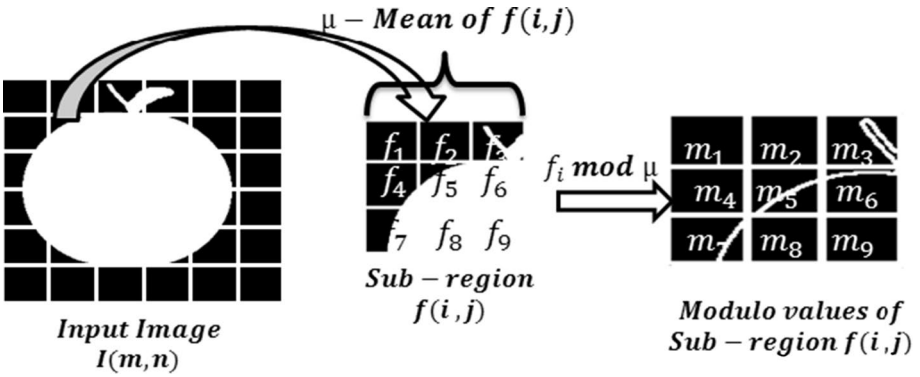

Fig. 2 Formation of MA image

directional indices are assigned a decimal code replacing the center pixel, thereby; representing each shape as a collection of LAPD codes as represented in Fig. 3.

The encoding mechanism commences with the selection of $n \times n$ region, from the given image I, where 'n' takes only odd values. Later, the directionalized absolute pixel differences $D_0, D_1, D_2, D_3, D_4, D_5, D_6, D_7$ having 45° separation is evaluated in local

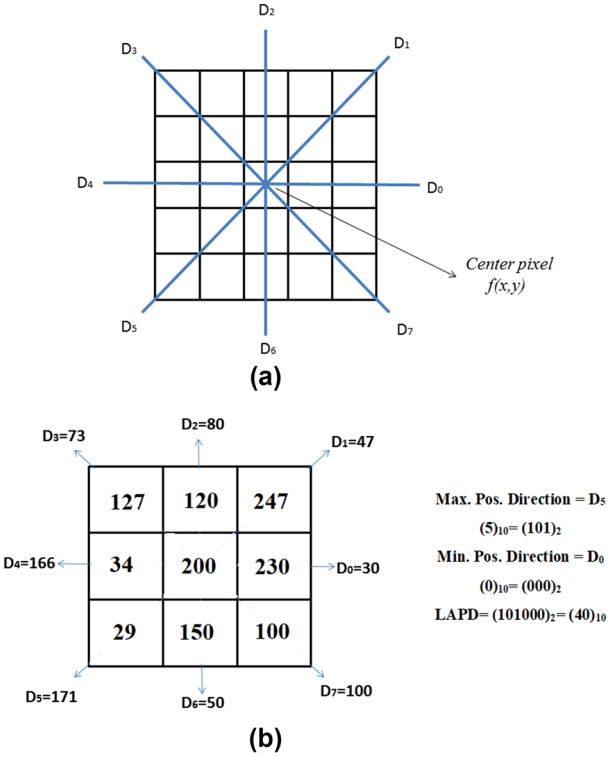

Fig. 3 LAPD code generation **a** For a given block $n \times n$ with directions $D_0, D_1, D_2, D_3, D_4, D_5, D_6$ and D_7 **b** Example for 3×3 block

neighborhood as illustrated in Fig. 3a. The center pixel of $n \times n$ mask is denoted as $f(x, y)$ and the LAPDs along each direction are evaluated using Eqs. (1) to (8).

$$D_0(x,y) = \sum_{i=0}^{\frac{n}{2}-1} |f(x,y+i) - f(x,y+i+1)| \tag{1}$$

$$D_1(x,y) = \sum_{i=0}^{\frac{n}{2}-1} |f(x-i,y+i) - f(x-i-1,y+i+1)| \tag{2}$$

$$D_2(x,y) = \sum_{i=0}^{\frac{n}{2}-1} |f(x-i,y) - f(x-i-1,y)| \tag{3}$$

$$D_3(x,y) = \sum_{i=0}^{\frac{n}{2}-1} |f(x-i,y-i) - f(x-i-1,y-i-1)| \tag{4}$$

$$D_4(x,y) = \sum_{i=0}^{\frac{n}{2}-1} |f(x,y-i) - f(x,y-i-1)| \tag{5}$$

$$D_5(x,y) = \sum_{i=0}^{\frac{n}{2}-1} |f(x+i,y-i) - f(x+i+1,y-i-1)| \tag{6}$$

$$D_6(x,y) = \sum_{i=0}^{\frac{n}{2}-1} |f(x+i,y) - f(x+i+1,y)| \tag{7}$$

$$D_7(x,y) = \sum_{i=0}^{\frac{n}{2}-1} |f(x+i,y+i) - f(x+i+1,y+i+1)| \tag{8}$$

where $\lfloor \rfloor$ is floor value.

Upon determining the LAPD values amongst each pixel with its neighbours, the prominent pixel difference values are identified as shown in Fig. 3b, for a 3×3 neighbourhood. Amongst, the resulting values the index of the maximum absolute value and the minimum absolute value representing the directional numbers are concatenated for generating the LAPD code. Since, the directional indices are represented by numbers 0–7; the resulting directional indices occupy 3-bits each. The ensuing 6-bit LAPD code replaces the 8-bit pixels of a given image, thus reducing the memory. The LAPD code is mathematically formulated in Eq. (9).

$$LAPD_6(x,y) = \left\{ \bigcup [(i_{x,y})_{10}]_2, [(j_{x,y})_{10}]_2 \right\}_{10} \tag{9}$$

where concatenation is represented as ∪, with (x, y) denoting the pixel position. And the maximum, minimum directional value indices are represented as $i_{x,y}$,$j_{x,y}$ respectively as given in (10), (11) and $(K)_b$, $[k]_b$and$\{k\}_b$ is representation of K with respect to base b.

$$i_{x,y} = \arg max\{D_i(x, y), |0 \le i \le 7|\} \tag{10}$$

$$j_{x,y} = \arg min\{D_j(x, y), |0 \le j \le 7|\} \tag{11}$$

The space requirement is further exploited by LAPD in the form of a 3-bit LAPD code given by (12)

$$LAPD_3(x, y) = \left(\left|i_{x,y} - j_{x,y}\right|\right)_2 \tag{12}$$

where | | is absolute value, $i_{x,y}$ and $j_{x,y}$ are presented in (10) and (11) respectively.

Conventional mask sizes of $3 \times 3, 5 \times 5, 7 \times 7$ and 9×9 are considered in this work for formulating LAPD codes. The LAPD features are encoded in the range 1 to 62 thereby enriching the high frequency information, as well as the novel encoding method reduces the feature size.

2.2.1 Space Saving Mechanism

The space occupied by MA-LAPD feature is reduced by the simple and novel arrangement scheme as discussed below. For general representation, the maximum and minimum directional indices of LAPD occupy three bits each summing to a total of 6 bits. When considering real-time implementation, both the indices demand 8-bit each, thereby, totalling to 16 bits. To address this issue and restrict the number of bits to 8, a novel compaction mechanism is presented in Fig. 4. The 8-bits resulting from the maximum and minimum directions are compacted to 8-bits by performing the left shift operation of anyone directional number and then, taking the logical 'OR' operation. This operation significantly reduces the size of the descriptor to half, thereby, minimizing the LAPDs storage space. Thus, this

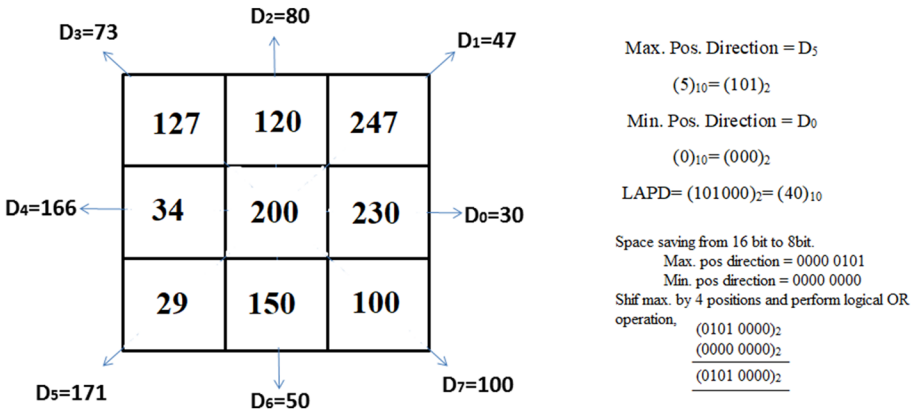

Fig. 4 Space saving mechanism

paper presents a novel shape descriptor scheme that considers the computational dimensions, particularly, when implemented in real-time.

2.3 Feature Representation

The resulting LAPD code matrix is then partitioned into fixed sub-matrices of size $p \times p$ from which the corresponding histograms are formulated and appended to finally yield the shape descriptor (s) mathematically depicted in equation Eq. (13).

$$s = [h_1 h_2 h_3 \ldots h_i] \tag{13}$$

where h is local histogram of each sub-region and $i = M/p$. This process is depicted in Fig. 5.

3 Evaluation of MA-LAPD

Efficiency of MA-LAPD is rigorously analysed with related validation metrics and is presented in below sections. Widespread shape datasets namely Kimia's 99, MPEG-7 CE Shape-1 Part B, TARI-1000 were utilized for effective testing of diverse descriptors addressing various shape characteristics. The popular Bull's Eye Retrieval (BER) [1] is employed in this work for analysing MA-LAPDs efficiency. To investigate MA-LAPD, a shape retrieval methodology is formulated by employing the supervised KNN classifier for shape classification. The image dataset is then parted into training, testing shapes for cross validation based on the number of folds for rendering an efficient data classification model.

The KNN training parameters used for the presented work are as follows: the number of observations (N) takes the dataset size as input. Likewise, the labels X and Y are loaded with the feature values in accordance with the dataset size. The distance metric is assumed

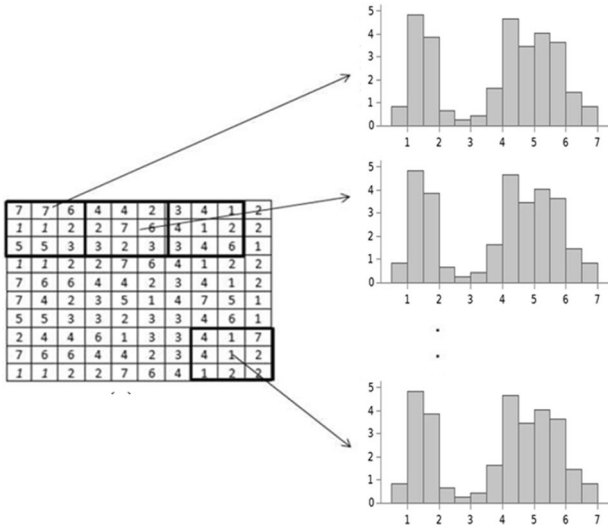

Fig. 5 Building shape histograms from the MA-LAPD data. **a** Tiling MA-LAPD features into 3×3 sub-regions **b** LAPD feature histograms

to be Euclidean and the number of neighbours is assumed as 2 for building the KNN classification model. Also, the hybrid clustering schemes detailed in [17–19] dealing with text-based retrieval assisted in extending the KNN classifier for shape classification owed to its classification accuracy. The retrieval mechanism is implemented in MATLAB R2015a software operating on an i3 CPU system clocking at 2 GHz and running on Windows7 platform. Detailed investigations on different dataset are performed and dealt under relevant headers.

3.1 MPEG-7 Dataset

This dataset is widely established amongst the schemes dealing with shape retrieval. An identified set of twenty images is distributed amongst 70 classes summing up to 1400 images that make up this dataset. This dataset is used in most of the shape retrieval framework listed in the literature [1, 6, 7, 20–23]. Figure 6 shows example shapes from each category of the MPEG-7dataset.

For BER analysis, initially the affinity matrix was constructed with the formulation of feature database during the offline phase. The shape histogram of the query is extracted and then mapped with the affinity matrix. Likewise, every other shape queries the dataset and is mapped with the other shapes. As discussed earlier, the KNN classifier is tuned by fivefold cross validation for improving the classification accuracy. Later, the 20 most similar shapes from each class belonging to the query are retrieved. Then, the matching shapes for all the queries belonging to each class are added and divided by the affinity matrix dimension to yield the BER.

3.1.1 Localisation Analysis

The consistency of LAPD efficiency is studied by individually constructing LAPD with variable masks of $3 \times 3, 5 \times 5, 7 \times 7$and 9×9 and analysing their BER. BER scores attained with variable LAPD mask sizes stated in Table 1 signify the localization potential of the blended MA and LAPD operations.

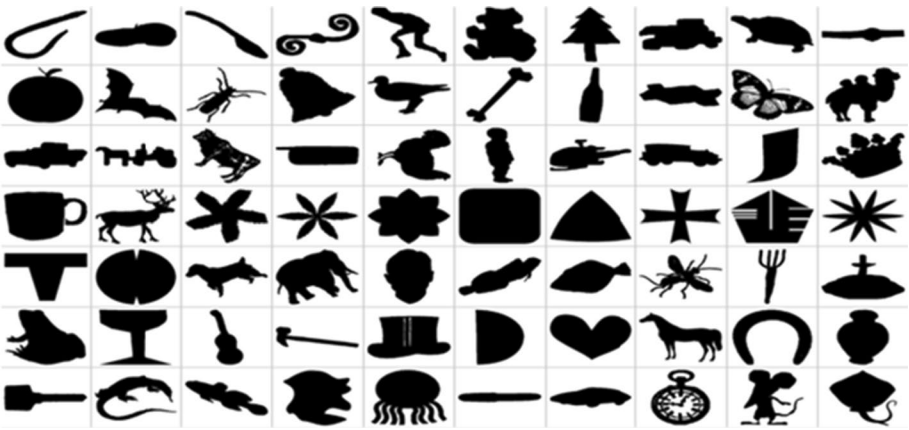

Fig. 6 Image samples from the MPEG-7

Table 1 BER score attained for different mask sizes on the MPEG-7 dataset

Mask sizes	BER rate (%)
3×3	95.03
5×5	95.36
7×7	95.50
9×9	95.65

For relative comparison the highest BER value reported for LAPD mask size in Table 1 is stated along with widely popular schemes in Table 2.

Although, lower mask sizes deliver consistent accuracy more than 95%, for relative comparison the 9×9 LAPD mask alone is considered in Table 2. The BER of MA-LAPD has surpassed its competitors as evident in Table 2. The above efficiency is clearly owed to the localization and congruent nature of the wrap-around operation introduced in the characterization. Later, LAPD has effectively encoded these directional variations to render fine shape descriptors. Moreover, this mechanism employs simple modules to achieve BER of 95.65, rather the schemes of [1, 5, 25, 26], deploying dynamic programming and fall behind MA-LAPD as witnessed in Table 2.

3.2 Tari-1000 Dataset

The main distinction between this dataset and the MPEG-7 lies in containing shapes with higher articulation variations. Thereby, attaining higher accuracy in Tari-1000 remains a challenge owing to the higher degree of intra-class shape deformations. The 1000 silhouette shapes of this dataset are organized as 50 classes with each class comprising 20 shapes. Example of shapes present in Tari-1000 dataset is illustrated in Fig. 7.

Table 2 BER comparison with existing shape retrieval methods in the MPEG7 dataset

Method	BER rate (%)
ECCobj2D [24]	54.56
SC [3]	64.59
IDSC [4]	68.63
Mean-EuDist [25]	77.69
IDSC + DP [4]	85.40
SC + DP [3]	86.60
Shape tree [26]	87.70
CBTA [1]	89.45
Height functions [27]	89.66
Shape vocabulary [10]	90.41
IMD [19]	91.25
CBTA + SC [1]	93.65
LTEM + hist [28]	94.64
HGTT [29]	95.09
TFD [23]	95.35
MA-LAPD$_{9\times9}$	95.65

Fig. 7 Shape examples in Tari-1000 dataset

As discussed above, the affinity matrix with LAPD histograms are evaluated and the KNN classification model is tuned for maintaining the accuracy. The validation procedure adopted in MPEG-7 dataset is extended here to analyse the MA-LAPD performance in Tari-1000. The regional (mask) size analysis performed in MPEG7 is repeated in this dataset and the attained BER values are reported in Table 3.

From Table 3, it is evident that varying mask sizes does not significantly impact the BER rates. Hence, for relative comparison, the 9×9 mask is chosen owing to its higher BER stated in Table 3. Table 4 depicts the relative retrieval rates of different retrieval mechanisms compared with MA-LAPD.

As witnessed in Table 4, the IDSC approach leads the other approaches with the highest BER score. This is because of the inherent point-wise matching operation present in IDSC that makes it articulation insensitive. Despite BER falling behind other descriptors MA-LAPD is able to maintain consistent BER greater than 91% in both these datasets which is unseen for its competitors as they fail to reproduce a similar performance in the others. This quality is mainly due to the multiple interactions happening amongst the localised pixels fused into this feature formulation mechanism.

Table 3 BER score for various mask sizes in Tari-1000 dataset

Mask sizes	BER rate (%)
3×3	93.41
5×5	93.50
7×7	93.71
9×9	93.92

Table 4 Relative BER comparison on TARI-1000

Scheme	BER rate (%)
LTEM + Hist [28]	91.70
SC [3]	94.17
IDSC [4]	95.33
ASC [20]	95.44
SC + LP [21]	97.79
TFD [23]	93.45
HGTT [29]	93.87
MA-LAPD$_{9\times9}$	93.92

3.3 Kimia's 99 Dataset

Another popular dataset that is commonly employed by several shape retrieval schemes is the Kimia's 99. Although the variants Kimia's 25, Kimia's 256 are available still Kimia's 99 is widely used for validation as several shapes belonging to the former dataset are encompassed in Tari-1000. Also, Kimias 25 is avoided in this analysis as it contains fewer shapes when compared with Kimia's 99. Few example shapes of Kimia's 99 are depicted in Fig. 8.

Kimia's 99 is organized into 9 classes with each class consisting of 11 images thereby, making a total of 99 shapes. Each shape of Kimia's 99 queries the retrieval scheme and the matched shapes ranking from top 1 to top 10 are retrieved and displayed in Fig. 9.

Figure 9 displays the matched retrievals from each class for a given query. Column 1 lists the different query images and the columns following it display the shapes ascendingly ranked from Top 1 to Top 10 with regard to the given query. Also, the misrecognized shapes are bounded using red boxes in the retrievals. This is mainly due to the sub-region matching of the query image with several other parts of other images belonging to another class due to local feature extraction. Table 5 shows the localization results of the presented framework with variable LAPD mask sizes of 3×3, 5×5, 7×7 and 9×9.

Although, lower mask sizes deliver consistent accuracy more than 93%, for relative comparison, LAPD mask with 9×9 is presented in Table 6. Table 6 compares MA-LAPD with its popular competitors namely, Shape Context (SC) [3], Inner Distance Shape Description (IDSC) [4], Mean-alignment Euclidean (Mean- EuDist) [12], Eccentricity Transform (ECCobj2D) [24] and Contour Points Distribution Histogram (CPDH) [22].

Table 6, apparently signifies the higher Top 1 result achieved by MA-LAPD with regard to the prevailing mechanisms. Also, MA-LAPD delivers highest BER even for the Top 10 rank and dominates the earlier schemes thereby, showcasing its effectiveness. An attribute

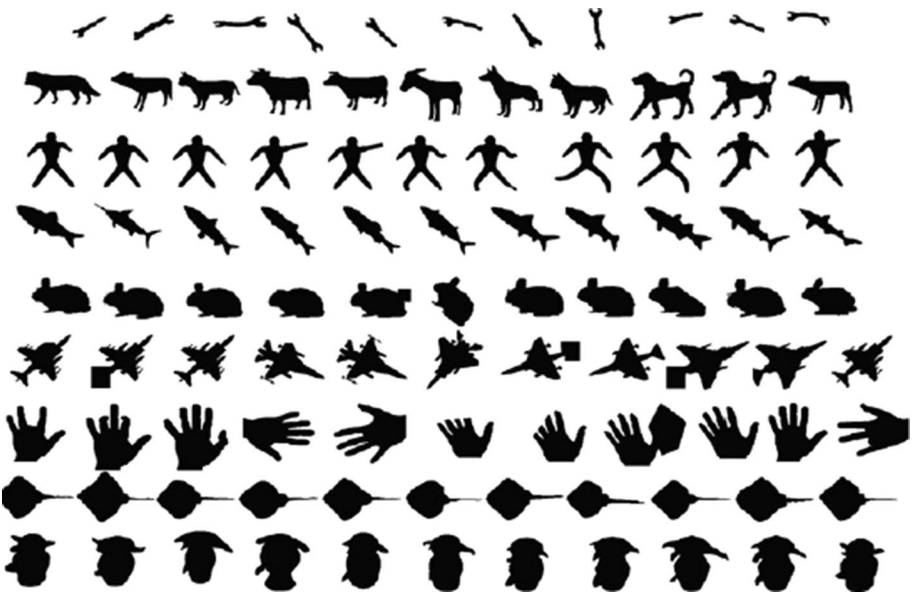

Fig. 8 Example shapes in Kimia's 99

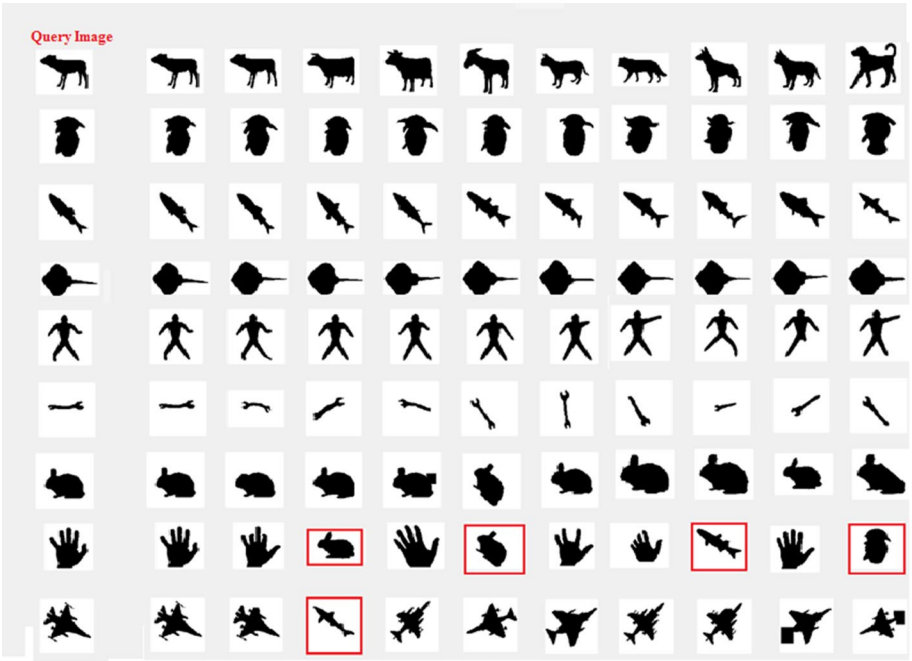

Fig. 9 Top-10 ranked retrievals on Kimia's 99

Table 5 BER values for different Mask sizes on the Kimia's 99 dataset

Mask size	1st	2nd	3rd	4th	5th	6th	7th	8th	9th	10th
3×3	99	98	98	93	96	92	87	89	90	82
5×5	99	98	98	93	94	92	88	90	90	74
7×7	99	98	96	94	94	92	88	90	89	81
9×9	99	98	98	94	95	94	94	93	91	87

Table 6 Top 1–Top 10 ordered BER values of different descriptors

Method	1st	2nd	3rd	4th	5th	6th	7th	8th	9th	10th
ECCobj2D [24]	94	85	81	73	81	73	64	59	56	35
SC [3]	97	91	88	85	84	77	75	66	56	37
Mean-DIR Euclidean [12]	97	92	89	86	81	80	74	74	70	52
CPDH [22]	98	94	95	92	90	88	85	84	71	52
LTEM + Hist [28]	99	99	96	94	87	86	85	80	82	78
IDSC + DP [4]	99	99	99	98	98	97	97	98	94	79
TFD [23]	99	98	97	96	94	95	94	93	93	84
HGTT [29]	99	98	98	94	95	94	94	93	91	87
MA - $LAPD_{9\times9}$	99	99	98	95	94	94	95	94	92	90

solely owed to the simple and acute shape characterization. Rather, others achieve it by utilizing complex dynamic programming. Furthermore, MA-LAPD robustness is well demonstrated in Fig. 9 that supplements the ability of the intended shape description.

4 Conclusion

A computationally light and novel shape descriptor labelled as Modulo Arithmetic-Local Absolute Pixel Differences (MA-LAPD) is contributed in this paper. The MA-LAPD descriptor of image sub-regions is constructed using modulo operation in an overlapping manner. The resulting image is then encoded using the novel LAPD packing mechanism to produce the MA-LAPD descriptor. Validations on the benchmark datasets establish MA-LAPD to be invariant towards diverse affine transformations which is evident in the achieved BERs. Computationally simple, consistent BER and superior performances witnessed across the different datasets signify MA-LAPDs potential. However, MA-LAPDs BER falls slightly in comparison with its peers if the shapes contain more articulation changes, a constraint that is to be addressed. Also, this concept can be extended to deal with large image database warranting rapid retrieval with improved retrieval accuracy. Extension of the presented descriptor to super-resolution retrieval applications remains the future scope.

References

1. Hu, D., Huang, W., Yang, J., Shang, L., & Zhu, Z. (2015). Shape matching and object recognition using common base triangle area. *IET Computer Vision, 9*(5), 769–778. https://doi.org/10.1049/iet-cvi.2014.0409.
2. Zhang, D., & Lu, G. (2004). Review of shape representation and description techniques. *Pattern Recognition, 37*(1), 1–19. https://doi.org/10.1016/j.patcog.2003.07.008.
3. Belongie, S., Malik, J., & Puzicha, J. (2002). Shape matching and object recognition using shape contexts. *IEEE Transactions on Pattern Analysis and Machine Intelligence, 24*(4), 509–522. https://doi.org/10.1109/34.993558.
4. Ling, H., & Jacobs, D. W. (2007). Shape classification using the inner-distance. *IEEE Transactions on Pattern Analysis and Machine Intelligence, 29*(2), 286–299. https://doi.org/10.1109/TPAMI.2007.41.
5. Alajlan, N., El Rube, I., Kamel, M. S., & Freeman, G. (2007). Shape retrieval using triangle-area representation and dynamic space warping. *Pattern Recognition, 40*(7), 1911–1920. https://doi.org/10.1016/j.patcog.2006.12.005.
6. Alajlan, N., Kamel, M. S., & Freeman, G. H. (2008). Geometry-based image retrieval in binary image databases. *IEEE Transactions on Pattern Analysis and Machine Intelligence, 30*(6), 1003–1013. https://doi.org/10.1109/TPAMI.2008.37.
7. De Souza, G. B., & Marana, A. N. (2013). HTS: A new shape descriptor based on Hough Transform. In *Proceedings—IEEE international symposium on circuits and systems* (pp. 974–977). https://doi.org/10.1109/ISCAS.2013.6572011.
8. Srestasathiern, P., & Yilmaz, A. (2011). Planar shape representation and matching under projective transformation. *Computer Vision and Image Understanding, 115*(11), 1525–1535. https://doi.org/10.1016/j.cviu.2011.07.004.
9. Wu, H., & Yan, S. (2016). Computing invariants of Tchebichef moments for shape based image retrieval. *Neurocomputing, 215,* 110–117. https://doi.org/10.1016/j.neucom.2015.05.147.
10. Bai, X., Rao, C., & Wang, X. (2014). Shape vocabulary: A robust and efficient shape representation for shape matching. *IEEE Transactions on Image Processing, 23*(9), 3935–3949. https://doi.org/10.1109/TIP.2014.2336542.
11. Matsuda, Y., Ogawa, M., & Yano, M. (2015). Shape retrieval with geometrically characterized contour partitions. *IEEE Access, 3,* 1161–1178. https://doi.org/10.1109/ACCESS.2015.2451627.

12. Kaothanthong, N., Chun, J., & Tokuyama, T. (2016). Distance interior ratio: A new shape signature for 2D shape retrieval. *Pattern Recognition Letters, 78,* 14–21. https://doi.org/10.1016/j.patrec.2016.03.029.
13. Mukhopadhyay, A., Mukherjee, I., & Biswas, P. (2019). Comparing shape descriptor methods for different color space and lighting conditions. *Artificial Intelligence for Engineering Design, Analysis and Manufacturing: AIEDAM, 33*(4), 389–398. https://doi.org/10.1017/S0890060419000398.
14. Mostafa, Y. (2020). A new shape descriptor for road network separation from parking lots and intersection detection on VHR remote sensing images. *International Journal of Remote Sensing, 41*(11), 4226–4237. https://doi.org/10.1080/01431161.2020.1714780.
15. Elmezain, M., & Ibrahem, H. M. (2020). OUP accepted manuscript. *The Computer Journal*. https://doi.org/10.1093/comjnl/bxaa118.
16. Bai, X., Yang, X., Latecki, L. J., Liu, W., & Tu, Z. (2010). Learning context-sensitive shape similarity by graph transduction. *IEEE Transactions on Pattern Analysis and Machine Intelligence, 32*(5), 861–874. https://doi.org/10.1109/TPAMI.2009.85.
17. Abualigah, L. M., & Khader, A. T. (2017). Unsupervised text feature selection technique based on hybrid particle swarm optimization algorithm with genetic operators for the text clustering. *Journal of Supercomputing, 73*(11), 4773–4795. https://doi.org/10.1007/s11227-017-2046-2.
18. Abualigah, L. M. Q. (2019). Feature selection and enhanced krill herd algorithm for text document clustering. *Studies in Computational Intelligence, 816,* 1–186. https://doi.org/10.1007/978-3-030-10674-4.
19. Abualigah, L. (2020). Multi-verse optimizer algorithm: A comprehensive survey of its results, variants, and applications. *Neural Computing and Applications*. https://doi.org/10.1007/s00521-020-04839-1.
20. Yang, J., Wang, H., Yuan, J., Li, Y., & Liu, J. (2016). Invariant multi-scale descriptor for shape representation, matching and retrieval. *Computer Vision and Image Understanding, 145,* 43–58. https://doi.org/10.1016/j.cviu.2016.01.005.
21. Ling, H., Yang, X., & Latecki, L. J. (2010). Balancing deformability and discriminability for shape matching. In *Lecture notes in computer science (including subseries lecture notes in artificial intelligence and lecture notes in bioinformatics)* (Vol. 6313 LNCS, pp. 411–424). Springer. https://doi.org/10.1007/978-3-642-15558-1_30.
22. Shu, X., & Wu, X. J. (2011). A novel contour descriptor for 2D shape matching and its application to image retrieval. *Image and Vision Computing, 29*(4), 286–294. https://doi.org/10.1016/j.imavis.2010.11.001.
23. Priyanka, S., & Sudhakar, M. S. (2018). Tetrakis square tiling-based triangulated feature descriptor aiding shape retrieval. *Digital Signal Processing: A Review Journal, 79,* 125–135. https://doi.org/10.1016/j.dsp.2018.04.012.
24. Ion, A., Artner, N. M., Peyré, G., Kropatsch, W. G., & Cohen, L. D. (2011). Matching 2D and 3D articulated shapes using the eccentricity transform. *Computer Vision and Image Understanding, 115*(6), 817–834. https://doi.org/10.1016/j.cviu.2011.02.006.
25. Jomma, H. D., & Hussein, A. I. (2016). Circle views signature: A novel shape representation for shape recognition and retrieval. *Canadian Journal of Electrical and Computer Engineering, 39*(4), 274–282. https://doi.org/10.1109/CJECE.2016.2574745.
26. Felzenszwalb, P. F., & Schwartz, J. D. (2007). Hierarchical matching of deformable shapes. In *Proceedings of the IEEE computer society conference on computer vision and pattern recognition*. https://doi.org/10.1109/CVPR.2007.383018.
27. Wang, J., Bai, X., You, X., Liu, W., & Latecki, L. (2012). Shape matching and classification using height functions. *Pattern Recognition Letters, 33,* 134–143.
28. Govindaraj, P., & Sudhakar, M. S. (2018). Shape characterization using laws of texture energy measures facilitating retrieval. *The Imaging Science Journal, 66*(2), 98–105. https://doi.org/10.1080/13682199.2017.1380356.
29. Govindaraj, P., & Sudhakar, M. S. (2018). Hexagonal grid based triangulated feature descriptor for shape retrieval. *Pattern Recognition Letters, 116,* 157–163. https://doi.org/10.1016/j.patrec.2018.10.004.

Kethepalli Mallikarjuna serves the Department of Electronics and Communication Engineering as the Professor with extensive research and teaching experience. Also, a consistent track record in publications with papers published in highly reputed journals.

Bepar Abdul Raheem serves the Department of Electronics and Communication Engineering as the Professor. Additionally, he holds the post of Dean, Professional Bodies and Non statutory Bodies. The author has high repute as an academician and researcher in the relevant fields.

Govindaraj Pathanadka has recently completed Post-Doctoral research from IIT Guwahati and has currently joined an engineering college as an Associate Professor. The author has a decent number of publications in reputed journals.

Sudhakar Moggapair Suriyakumar serves the Vellore Institute of Technology as an Associate Professor in the School of Electronics Engineering. The author has served industries, academic institutes and has a decent publication profile in the area of repute.